

FULL PAPER

Novel molecular switches based on viologen ligand and its transition metal complexes

Israa A. Jassem^{a,b,*}  | Wathiq S. Abdul-Hassan^a  | Ibrahim A. Flafel^a ^aDepartment of Chemistry, College of Science, University of Thi-Qar, 64001 Nassiria, Iraq^bDepartment of Pathological, College of Science, University of Sumer, Iraq

In this work, the viologen derivative was prepared by reacted of bis (3-chloroacetylacetone) ethylenediimine (AN-Cl) with mono-methylviologen (C_1V^+). The switching motion between dicationic viologen compound $C_1V^{2+}AN-Cl.2PF_6^-$ and diamagnetic intermolecular π -dimer ($C_1V^+AN-Cl. PF_6^-$)₂ was triggered through the reduction by 1 electron/viologen unit. This molecular switch was followed by UV-Visible absorption spectrometry. The viologen compound $C_1V^{2+}AN-Cl.2PF_6^-$ was titrated with Zn^{2+} , Cu^{2+} , Co^{2+} , and Fe^{2+} ions to afford metal complexes in the solution of $M^{2+}-C_1V^{2+}AN-Cl.2PF_6^-$. Moreover, four molecular switches were attained from those metal complexes ($M^{2+}-C_1V^+AN-Cl. PF_6^-$)₂ by the chemical reduction stimuli including the characterization of complexes of $M^{2+}-C_1V_1^{2+}AN-Cl.2PF_6^-$ were performed by UV-Visible absorption spectroscopy. It was noticed that ratio of metal to the ligand in the complexes of Zn^{2+} , Cu^{2+} , Co^{2+} , and Fe^{2+} was 1:1. Switching properties of the novel viologen derivatives with intermolecular dimer were studied by the reduction with activated zinc powder and followed by the absorption spectroscopy. After the 1e- reduction viologen unit in $C_1V_1^{2+}AN-Cl.2PF_6^-$ and $M^{2+}-C_1V_1^{2+}AN-Cl.2PF_6^-$, intermolecular dimerized viologen radicals occurred.

***Corresponding Author:**

Israa A. Jassem

E-mail: wathiq.a_chem@sci.utq.edu.iq

Tel.: +09627810015434

KEYWORDSBis (3-chloroacetylacetone) ethylenediimine; 4,4'-bipyridine; Viologen; Intermolecular π -dimerized $C_1V^{2+}AN-Cl.2PF_6^-$.**Introduction**

Viologens are organic salts of bipyridines quaternized at one or two nitrogen atoms. If the two substituents at two nitrogen atoms are the same, they are called 1,1'-disubstituted-4,4'-bipyridinium salts; if they are different, they are called 1-substituent-1'-substituent'-4,4'-bipyridinium salts.

When both substituents are methyl groups, the resulting dicationic molecule is known as methyl viologen. It was discovered to be an effective herbicide after being

studied as a redox indicator in biological investigations. Michaelis discovered the term "viologen" in 1933 after observing the violet color that resulted from the reduction of 1,1'-dimethyl-4,4' bipyridinium salt (DMV2+) by one electron to generate a radical cation (as a dimer) [1].

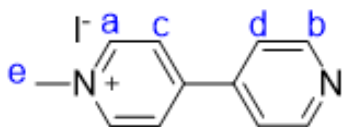
Viologens had been widely used as an antibacterial agent or herbicides. They are used, for example, as an active element in electrical display devices, diodes and transistors, memory devices, and molecular machine, electrodes for supercapacitors and

batteries catalysts for hydrogen production and gas storage and separation, pigments for sensitizing solar cells.

The main characteristics of viologens that make them important and essential building blocks for many materials can be summarized as follows: reduction of viologens to colored positive free radicals, and then to neutral species that can occur sequentially and reversibly within accessible potentials. Three oxidation states of cationic state radical cation and neutral state are and thermodynamically stable.

Experimental

Synthesis of 1-methyl-4,4'-bipyridinium (C_1V^+) [2]



Methyl iodide (0.39 mL, 6.4 mmol) was added with stirring into a solution of 4, 4'-bipyridine (1gm, 6.4 mmol) in 10 mL of dichloromethane, and then the solution was stirred at room temperature for 24 hours. The produced precipitate was collected by filtration, washed with dichloromethane and diethylether, recrystallized from methanol, and then dried under vacuum to afford $C_1V^+.I^-$ as a yellowish-orange precipitate, yield: 67%. M.p= 252 °C.

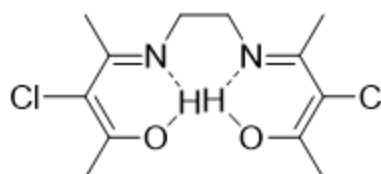
$C_1V^+.I^-$, 1H -NMR (500 MHz, DMSO- d_6), δ (ppm): 9.16 (d, $J = 6.1$ Hz, 2H, Ha), 8.86 (d, $J = 4.9$ Hz, 2H, Hb), 8.63 (d, $J = 6.1$ Hz, 2H, Hc), 8.04 (d, $J = 4.9$ Hz, 2H, Hd), and 4.40 (s, 3H, He).

Anion exchange

From Iodide forms to hexafluorophosphate form, the $C_1V^+.I^-$ was dissolved in the

minimum volume of distilled water. Upon the addition of saturated aqueous KPF_6 to the previous solution, the hexafluorophosphate salt of viologen derivative has been precipitated. The precipitate was collected by filtration and washed with distilled H_2O to afford the PF_6^- form: $C_1V^+.PF_6^-$ as a white precipitate.

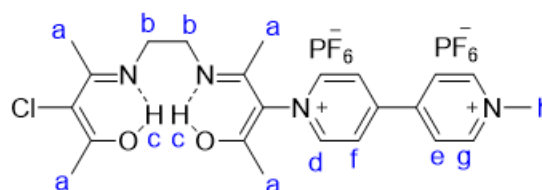
Synthesis of bis (3-chloroacetylacetonato) ethylenediimine (AN-Cl)[3]



Ethylenediamine (0.6 mL, 0.5315 g) in 2 ml ethanol was added gradually to 3-chloro acetylacetonate (2 mL, 2.38 g) in 2 mL ethanol placed in ice bath. The resulting mixture was stirred at room temperature for 24 h. The reaction progress was controlled by TLC (eluent = 4:1 Methanol: Benzene). The reaction mixture was left to dry under air atmosphere, and then under vacuum at room temperature.

The produced precipitate was washed with distilled water, m.p. 134 °C, yield 71.8 %.

Syntheses of final viologen derivative of $C_1V^{2+}AN-Cl.2PF_6^-$



$C_1V^+.I^-$ (1 gm, 3.35 mmol) was dissolved in DMF with stirring. When the solution becomes clear, AN-Cl (0.98 gm, 3.35 mmol) was added to the solution and the reaction.

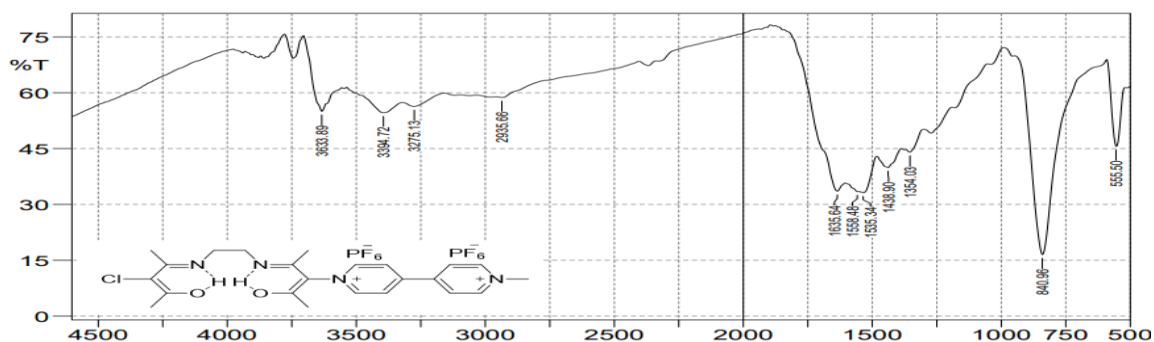


FIGURE 1 FT-IR spectrum of $C_1V^{2+}AN-Cl.2PF_6^-$

TABLE 1 FTIR data of $C_1V^{2+}AN-Cl.2PF_6^-$

Wave number (cm^{-1})	Assignment
$C_1V^{2+}AN-Cl.2PF_6^-$	
3394, 3633	$\nu O-H$
3050	$\nu C-H$ of aromatic and olefinic $C=C-H$
2935	aliphatic $\nu C-H$
1635	$\nu C=N$
1558	$\nu C=C$
1354	aliphatic $C-H$ bending
1296	$\nu C-O$
840	Aromatic and olefinic $C=C-H$ bending and νPF_6^-
555	$\nu C-Cl$

Thermal analysis of $C_1V^{2+}AN-Cl.2PF_6^-$ ligand

The Thermal behavior of $C_1V^{2+}AN-Cl.2PF_6^-$ thermal gravimetric analysis (TGA) was used to study the ligand, which was recorded in nitrogen gas at a constant heating rate of 15 $^{\circ}C/min$. The decomposition pattern of $C_1V^{2+}AN-Cl.2PF_6^-$ ligand occurs in three phases, as displayed in Figure 2 and Table 2. The following were these phases: the initial phase of $C_1V^{2+}AN-Cl.2PF_6^-$ starts at 45.99 $^{\circ}C$

and end at 101.17 $^{\circ}C$ with weight loss of 4.538%. This first stage includes the loss of two water molecule. The following phase begins at 196.37 $^{\circ}C$ and end at 344.92 $^{\circ}C$ which correspond to the losses of PF_6^- and methyl group. The final phase begins at 345.97 $^{\circ}C$ and ends at 599.39 $^{\circ}C$ and is due to the loss of ethylenediamine and chlorine atom and this correspond to weight loss of 15.588% [19].

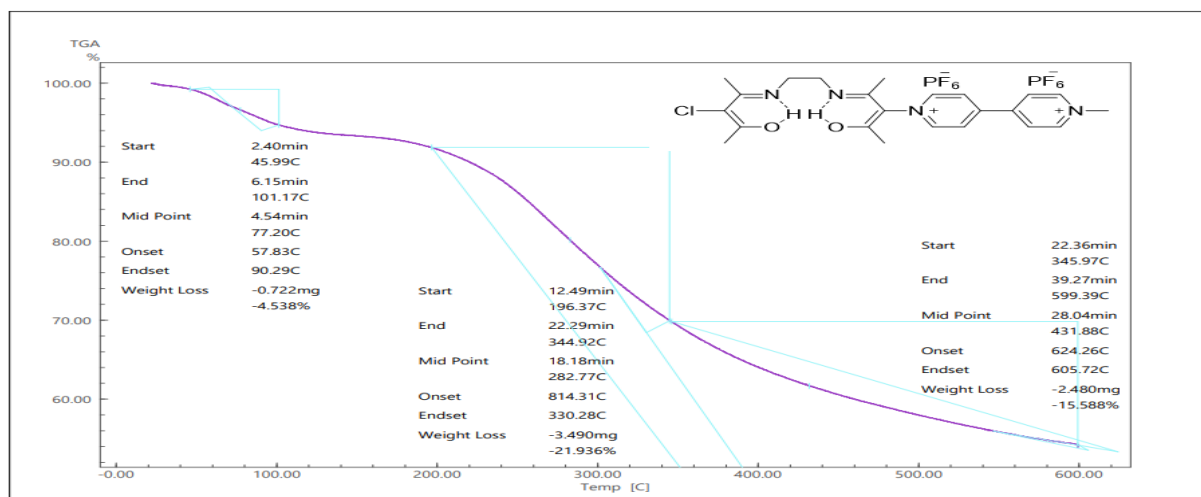


FIGURE 2 Thermal gravimetric analysis curve of $C_1V_2+AN-Cl.2PF_6^-$

TABLE 2 Thermal analyses data of $C_1V_2+AN-Cl.2PF_6^-$

Ligand	Temperature range °C	Weight loss %		Decomposition product
$C_1V_2+AN-Cl.2PF_6^-$	45.99-101.17	Found	Calculated	$2H_2O$
		4.538	5.012	
	196.37-344.92	21.936	22.2	PF_6+CH_3
	345.97-599.39	15.588	13.29	$NH_2CH_2CH_2NH_2+Cl$

Determination of rate constants, half-lives, and thermodynamic parameters using TG analyses

All thermal analysis stages can be considered as first order reactions. Therefore, using the first-order reaction rate equation, activation energy and other thermodynamic parameters were determined for all phase transformations [20].

$$\ln(1-x) = -kt \quad (1)$$

Equation 1 is plotted (time is x-axis and $\ln(1-x)$ is y-axis) and each line's slope provides the rate constant (k) for a specific TG phase, (Figures 3-5), and then the half-life time ($t_{1/2}$) was determined using Equation 2. Table 3 indicates values of k and $t_{1/2}$.

$$t_{1/2} = 0.693/k \quad (2)$$

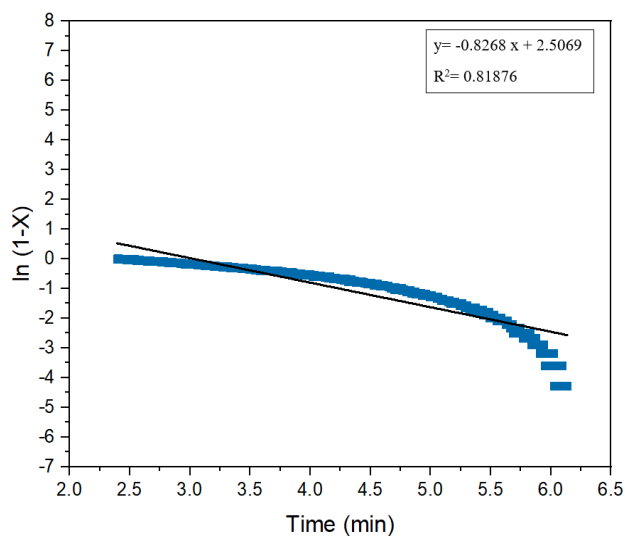


FIGURE 3 Plot of $\ln(1-x)$ vs. time for phase 1 of $C_1V_2^+AN-Cl.2PF_6^-$

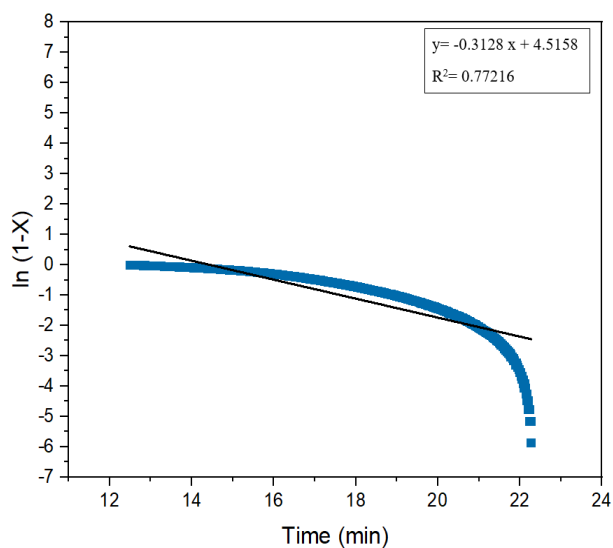


FIGURE 4 Plot of $\ln(1-x)$ vs. time for phase 2 of $C_1V_2^+AN-Cl.2PF_6^-$

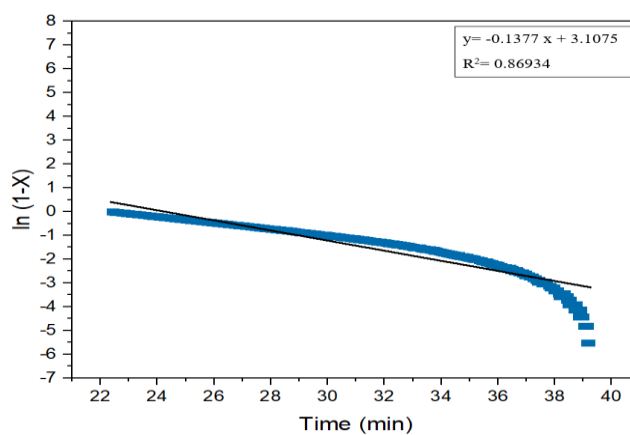


FIGURE 5 Plot of $\ln(1-x)$ vs. time for phase 3 of $C_1V_2^+AN-Cl.2PF_6^-$

Equation 3 illustrates how to determine kinetic parameters using a modified Coats and Redfern model [21-23]:

$$\ln [-\ln(1-x)] = \ln \frac{A}{RT^2} - \frac{E_a}{RT} \quad (3)$$

Where, β is the heating rate (10 °C/min and 20 °C/min), A is the pre-exponential factor, R is general gas constant (8.3143 Jmol⁻¹K⁻¹), E_a is the activation energy, and T is the

temperature (K). The activation energy is calculated by plotting graphs of $\ln[-\ln(1-x)]$ against $1000/T$ for each TG phase (Figures 6-8). Further thermodynamic parameters (ΔH , ΔS , and ΔG) are calculated using basic thermodynamic equations [24,25]. Values obtained for each phase (Table 3) proved that all TG phases are non-spontaneous (positive ΔG values) endothermic (positive ΔH values) reactions.

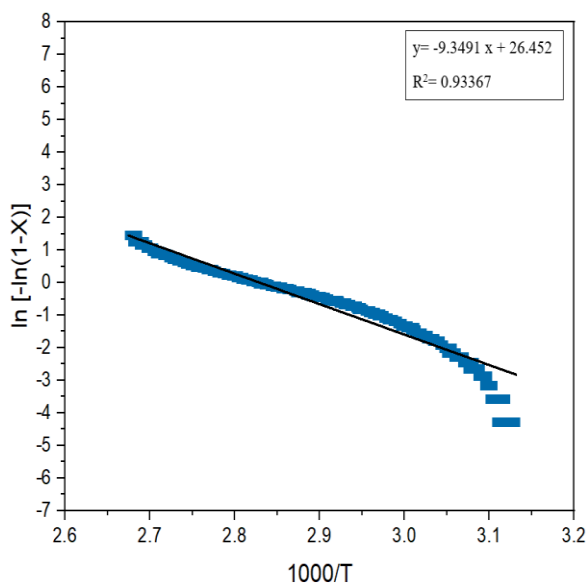


FIGURE 6 Plot of $\ln [-\ln (1-x)]$ vs. $1000/T$ for phase 1 of $C_1V_2+AN-Cl.2PF_6$

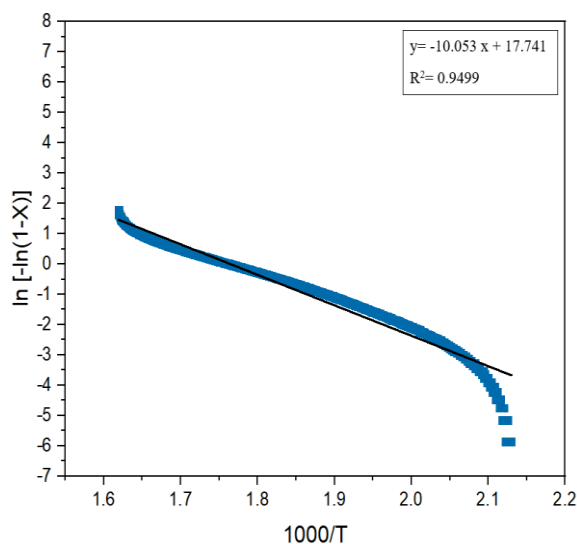


FIGURE 7 Plot of $\ln [-\ln (1-x)]$ vs. $1000/T$ for phase 2 of $C_1V_2+AN-Cl.2PF_6$

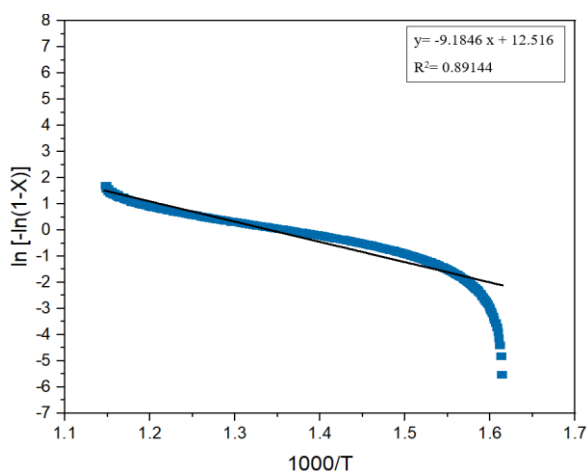


FIGURE 8 Plot of $\ln [-\ln (1-x)]$ vs. $1000/T$ for phase 3 of $C_1V^{2+}AN-Cl.2PF_6^-$

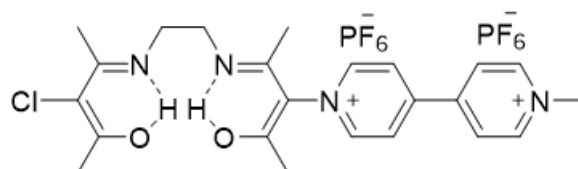
TABLE 3 Kinetic and thermodynamic parameters of each phase during thermogravimetric analysis of $C_1V^{2+}AN-Cl.2PF_6^-$

Compound	Phase	Temp. (K)	K (min^{-1})	$t_{1/2}$ (min)	Ea (Jmol^{-1}) $\times 10^4$	ΔH (Jmol^{-1}) $\times 10^4$	ΔS ($\text{Jmol}^{-1}\text{K}^{-1}$)	ΔG (Jmol^{-1}) $\times 10^4$
$C_1V^{2+}AN-Cl.2PF_6^-$	1	318.99	0.8268	0.8382	7.7731	7.5079	-56.916	9.3234
	2	469.37	0.3128	2.2155	8.3583	7.9681	-138.37	14.4629
	3	618.98	0.1377	5.0327	7.6363	7.1217	-189.46	18.8493

The reduction of $C_1V^{2+}AN-Cl.2PF_6^-$ ligand

For the first time, $C_1V^{2+}AN-Cl.2PF_6^-$ was interestingly reduced by solvation only in DMF to afford the intermolecular dimerized

viologen radicals of $C_1V^{2+}AN-Cl.2PF_6^-$ [26,27]. Also, the reduction was performed by activated zinc powder. Figure 9 illustrates the reduced $C_1V^{2+}AN-Cl.2PF_6^-$ by DMF and activated zinc powder.



$C_1V^{2+}AN-Cl.2PF_6^-$

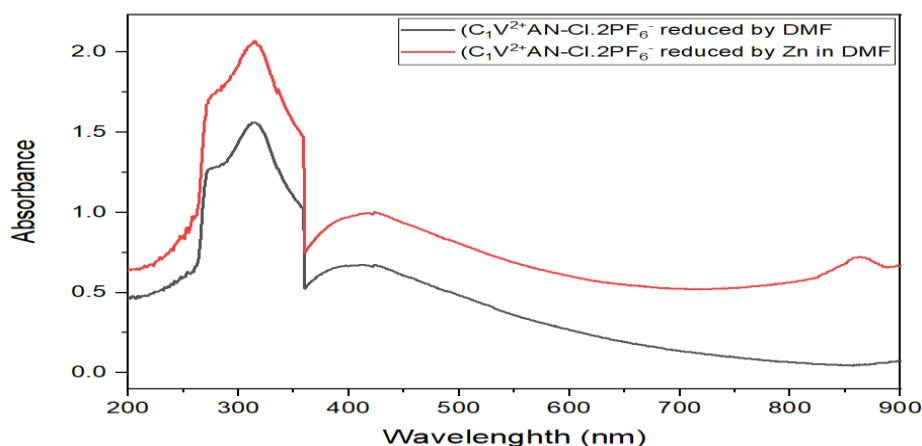


FIGURE 9 The UV-Visible absorption spectra of 0.1 mM $C_1V^{2+}AN-Cl.2PF_6^-$ reduced by DMF solvent (black line) and activated zinc powder (red line) at r.t. using quartz cell with a path length of 1 cm.

TABLE 4 The UV-Visible absorption data of 0.1mM $C_1V^{2+}AN-Cl.2PF_6^-$ reduced by DMF and activated zinc powder

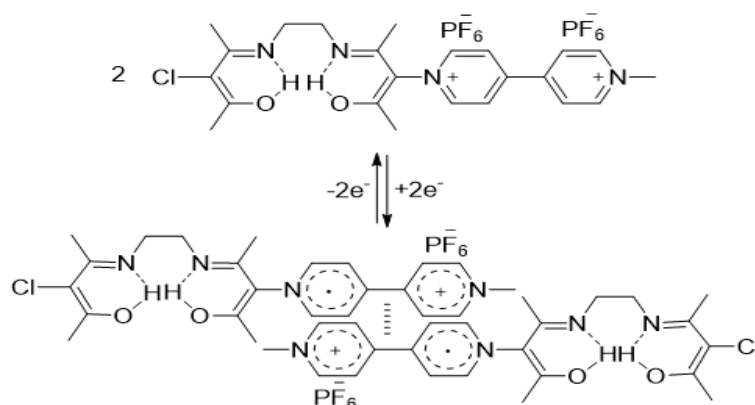
Wavelength (nm)	Absorbance at reduction by DMF	Absorbance at reduction by activated zinc powder in DMF
272	1.286	1.671
315	1.56	2.069
358	1.033	1.486
424	0.674	1.001
860	0.047	0.718

At dissolving $C_1V^{2+}AN-Cl.2PF_6^-$ in DMF, purple solution is obtained. This novel result refers that $C_1V^{2+}AN-Cl.2PF_6^-$ molecules have been reduced by only solvation to viologen $C_1V^{1.2+}AN-Cl.2PF_6^-$ that quickly and spontaneously π -dimerized to $(C_1V^{1.2+}AN-Cl.2PF_6^-)_2$. The absorption bands occurred at 358 nm and 424 nm at dissolving in DMF are assigned to dimerized and non-dimerized viologen radicals of $C_1V^{2+}AN-Cl.2PF_6^-$ (Figure 9, black spectrum and Table 4).

At reduction by activated zinc powder, deeper purple solution has been obtained compared with solution in DMF only. This

indicates to more reduction happened by activated zinc powder which is meaning more formation of intermolecular π -dimer among radical viologens.

Therefore, all absorptions after reduction by activated zinc powder have notably increased. The absorption peak at 424 nm is attributed to viologen radicals $C_1V^{1.2+}AN-Cl.2PF_6^-$ and those noted at 358 nm and 860 nm are absolutely related to formation of intermolecular π -dimer of viologen radicals, i.e. formation of $(C_1V^{1.2+}AN-Cl.2PF_6^-)_2$ species (Figure 9 (red line), Table 4, and Scheme 1).



SCHEME 1 Intermolecular π -dimerized $C_1V^{2+}AN-Cl.2PF_6^-$ by DMF and activated zinc powder in DMF

Reduction of Zn^{2+} , Cu^{2+} , Co^{2+} , and Fe^{2+} - $C_1V^{2+}AN-Cl.2PF_6^-$ complexes

The transition metals complexes of $C_1V^{2+}AN-Cl.2PF_6^-$ have been formed after addition 1 equivalent of tetrafluoroborate salts of Fe^{2+} , Co^{2+} , Cu^{2+} , and Zn^{2+} in DMF. The viologen units

within these complexes are also reduced by solvation in DMF and activated zinc powder. The spectra of these reduced compounds' UV-Visible absorption solutions are shown in Figures 10-13. Their data are listed in Tables 5-8, respectively.

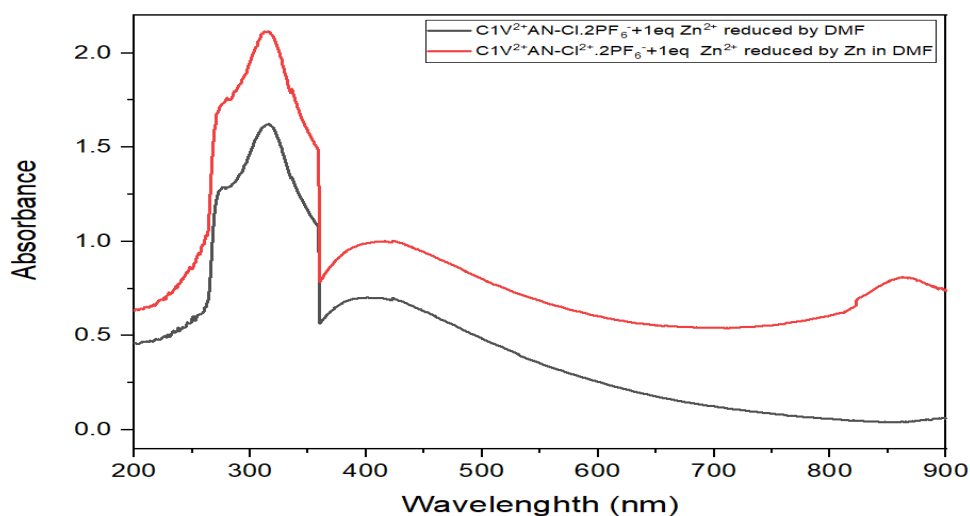


FIGURE 10 The UV-Visible absorption spectra of 0.1 mM $C_1V^{2+}AN Cl.2PF_6^-$ with 1eq of 0.1 mM $Zn(BF_4)_2.6H_2O$ reduced by DMF (black line) and activated zinc powder (red line) in DMF at r.t using quartz cell with a path length of 1 cm

TABLE 5 The UV-Visible absorption data of 0.1 mM $C_1V^{2+}AN-Cl.2PF_6^-$ with 1eq of Zn^{2+} by DMF and activated zinc powder in DMF

Wavelength (nm)	Absorbance at reduction by DMF	Absorbance at reduction by activated zinc powder in DMF
272	1.277	1.712
316	1.624	2.117
358	1.096	1.507
401	0.703	1.014
863	0.042	0.81

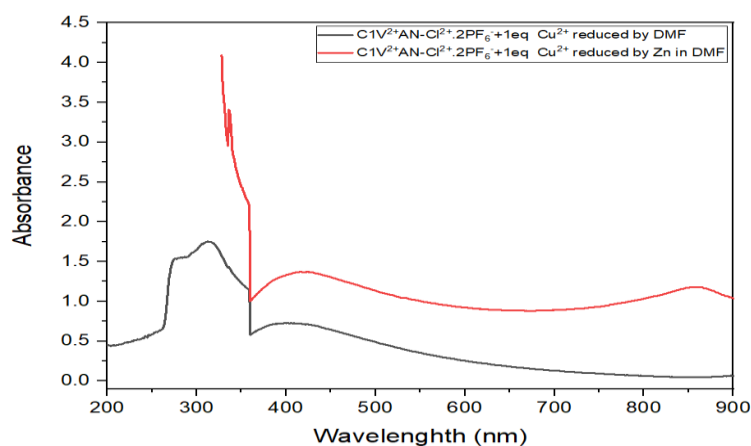


FIGURE 11 The UV-Visible absorption spectra of 0.1 mM $C_1V^{2+}AN Cl.2PF_6^-$ with 1eq of 0.1 mM $Cu(BF_4)_2.6H_2O$ reduced by DMF (black line) and activated zinc powder (red line) in DMF at r.t using quartz cell with a path length of 1 cm

TABLE 6 The UV-Visible absorption data of 0.1 mM $C_1V^{2+}AN Cl.2PF_6^-$ with 1eq of Cu^{2+} by DMF and activated zinc powder in DMF

Wavelength (nm)	Absorbance at reduction by DMF	Absorbance at reduction by activated zinc powder in DMF
274	1.584	Out of scale
312	1.624	Out of scale
358	1.150	Out of scale
405	0.727	1.375
858	0.048	1.514

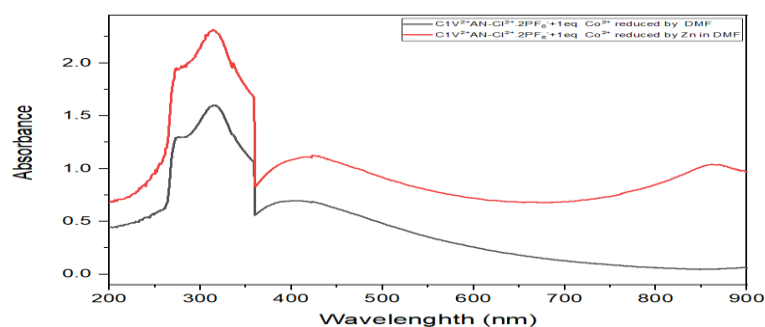


FIGURE 12 The UV-Visible absorption spectra of 0.1 mM $C_1V^{2+}AN Cl.2PF_6^-$ with 1eq of 0.1 mM $Co(BF_4)_2.6H_2O$ reduced by DMF (black line) and activated zinc powder (red line) in DMF at r.t using quartz cell with a path length of 1 cm

TABLE 7 The UV-Visible absorption data of 0.1 mM $C_1V^{2+}AN Cl.2PF_6^-$ with 1eq of Co^{2+} by DMF and activated zinc powder in DMF

Wavelength (nm)	Absorbance at reduction by DMF	Absorbance at reduction by activated zinc powder in DMF
273	1.331	1.959
317	1.602	2.317
358	1.069	1.692
405	0.696	1.126
862	0.049	1.041

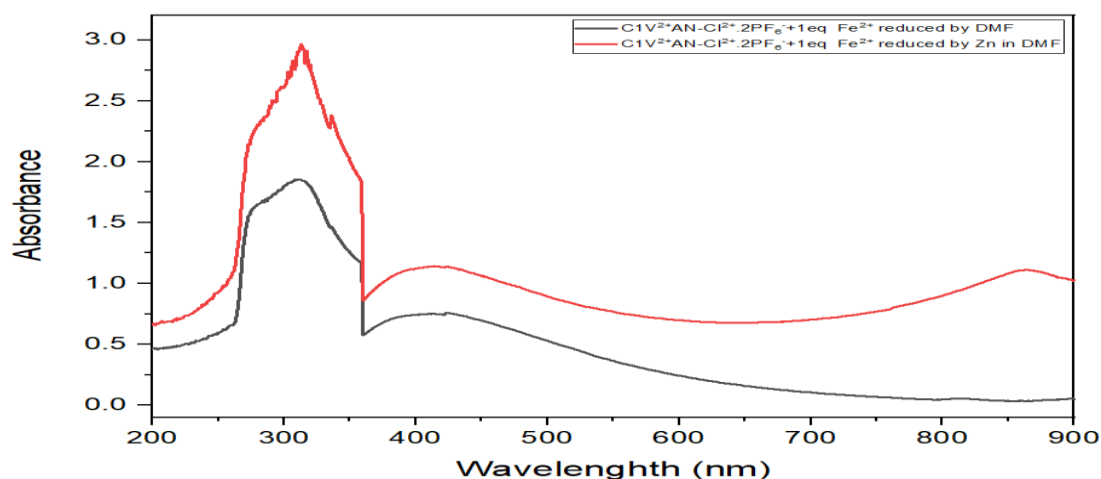


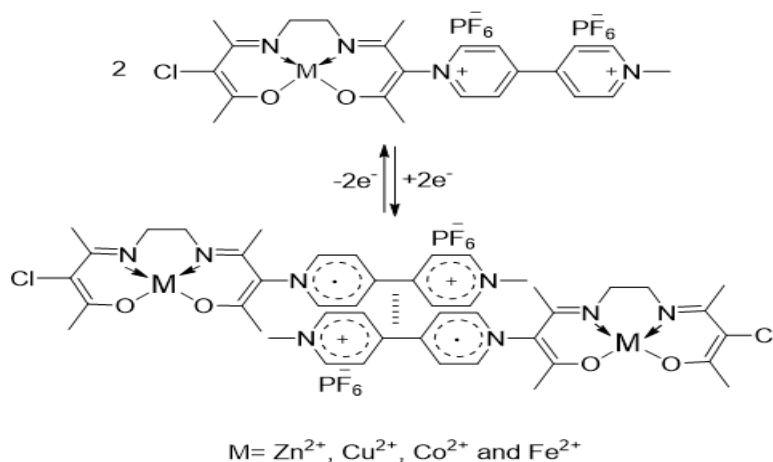
FIGURE 13 The UV-Visible absorption spectra of 0.1 mM $C_1V^{2+}AN.Cl.2PF_6^-$ with 1eq of 0.1 mM $Fe(BF_4)_2.6H_2O$ reduced by DMF (black line) and activated zinc powder (red line) in DMF at r.t using quartz cell with a path length of 1 cm

TABLE 8 The UV-Visible absorption data of 0.1 mM $C_1V^{2+}AN.Cl.2PF_6^-$ with 1eq of Fe^{2+} by DMF and activated zinc powder in DMF

Wavelength (nm)	Absorbance at reduction by DMF	Absorbance at reduction by activated zinc powder in DMF
273	1.548	2.123
313	1.853	2.966
358	1.168	1.856
423	0.759	1.142
862	0.035	1.111

The solutions of metal complexes with $C_1V^{2+}AN.Cl.2PF_6^-$ in DMF are also purple. This result indicates that the formation of complexes of $C_1V^{2+}AN.Cl.2PF_6^-$ with metal complexes does not prevent the interaction among viologen radicals to afford the intermolecular dimerization among two viologen radicals belonging to two metal complexes. The purple solutions of Fe^{2+} , Co^{2+} , Cu^{2+} , and Zn^{2+} complexes showed, respectively, the absorption bands 358 nm and 862 nm, 358 nm and 862 nm, 358 nm and 858 nm, and 358 nm and 863 nm. These absorption peaks are assigned to the

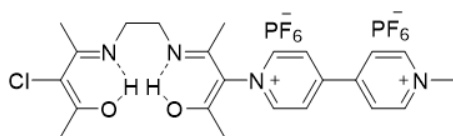
intermolecular π -dimerization among each two viologen radicals of two adjacent complexes [26-30]. The absorption peaks occurred at 423 nm, 405 nm, 405 nm, and 401 nm in absorption spectra of Fe^{2+} , Co^{2+} , Cu^{2+} , and Zn^{2+} complexes are attributed to non-dimerized viologen radicals [31-35]. The reduction of metal complexes by activated zinc powder resulted deeper purple solutions, i.e. increased absorbances at mentioned the maximum wavelengths. This is related to formation more viologen radicals, and then more π -dimers of these radicals, see Figures 10-14, Tables 5-8, and Scheme 2.



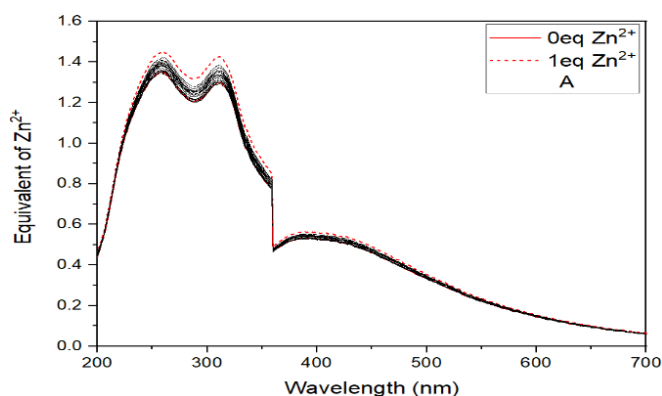
SCHEME 2 Intermolecular π -dimerized viologen radicals within metal complexes

UV-Visible absorption spectroscopy titration of $C_1V^{2+}AN-Cl.2PF_6^-$ with Zn^{2+} , Cu^{2+} and Fe^{2+} ions

The novel viologen compound $C_1V^{2+}AN-Cl.2PF_6^-$ was titrated using zinc tetrafluoroborate salts (II), copper (II), and iron (II) in ACN and followed by UV-Visible absorption spectroscopy, (Figures 3.20-3.22), respectively.



The spectrum of absorption of 0.07 mM $C_1V^{2+}AN-Cl.2PF_6^-$ was initially recorded. Secondly, the absorption spectrum was recorded after each addition of Zn^{2+} , Cu^{2+} , and Fe^{2+} ions to viologen compound solution. These spectra are demonstrated in Figures 3.14 (A), 3.15 (A), and 3.16 (A) respectively. Huge concentration of the titrant Zn^{2+} , Cu^{2+} and Fe^{2+} solution (50 mM) was used to avoid the effect of dilution during titration. The recorded absorptions of this solution was plotted versus added amount of Zn^{2+} , Cu^{2+} , and Fe^{2+} certain wavelengths and presented in Figures 14 (B and C), 15 (B and C), and 16 (B, C and D), respectively.



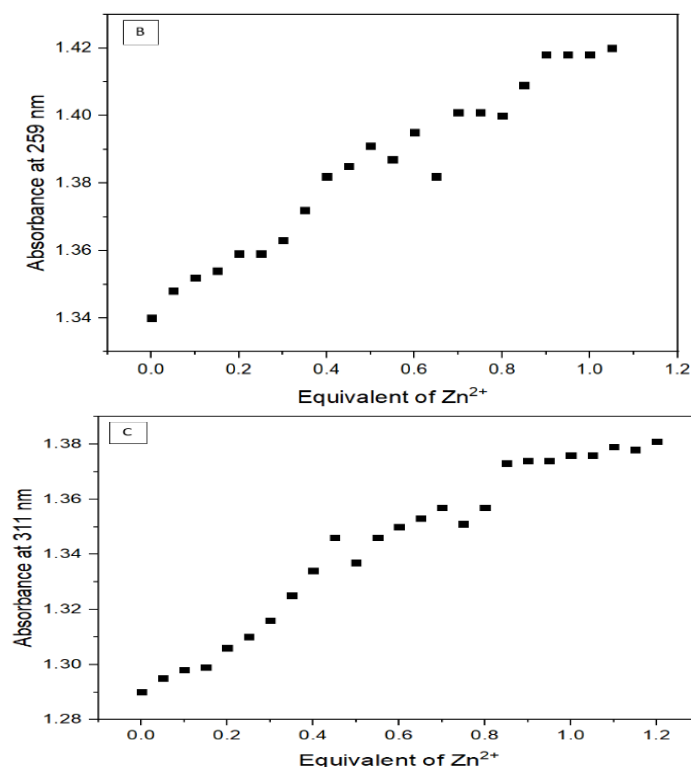


FIGURE 14 [A]: UV-visible absorption spectroscopy titration of 0.07 mM $C_1V^{2+}AN-Cl.2PF_6^-$ with 50 mM $[Zn(BF_4)_2.6H_2O]$ **[B], and [C]:** plots of absorbances at 259 nm and 311 nm, respectively, versus added equivalents of Zn^{2+} ion at r.t using quartz cell with a path length of 1 cm

The absorption spectra of $C_1V^{2+}AN-Cl.2PF_6^-$ with different equivalents of Zn^{2+} are presented in Figure 2.14 (A). The spectrum of 0.07 mM $C_1V^{2+}AN-Cl.2PF_6^-$ showed three absorption peaks in ACN which are noted at 259 nm, 311 nm, and 394 nm. These peaks could be attributed to ligand $C_1V^{2+}AN-Cl.2PF_6^-$ centered (LC, $\pi-\pi^*$, and $n-\pi^*$) [36] absorptions. Upon titration of $C_1V^{2+}AN-Cl.2PF_6^-$ with Zn^{2+} (formation of the complex: $Zn-C_1V^{2+}AN-Cl.2PF_6^-$), the intensities of these peaks increased gradually with the increase of the added amounts of the metal ion. This increase in peak intensities continues till the ratio of metal: ligand is 1:1, and then constant intensities are noted for several later

equivalents. Therefore, increased amounts of the complex have been formed before this ratio till getting the higher form of the complex at this ratio (Figures 14 (B and C) and Scheme 3) [37].

The 0.07 mM $C_1V^{2+}AN-Cl.2PF_6^-$ solution was titrated with 50 mM of $Cu(BF_4)_2.6H_2O$ in ACN and followed by absorption spectroscopy, as depicted in Figures 15 (A). The recorded absorptions at 258 nm and 312 nm of this solution against different amounts of added metal ions are plotted and presented in Figures 15(B and C). Similar notes and results appeared like those in the case of titration with Zn^{2+} ion.

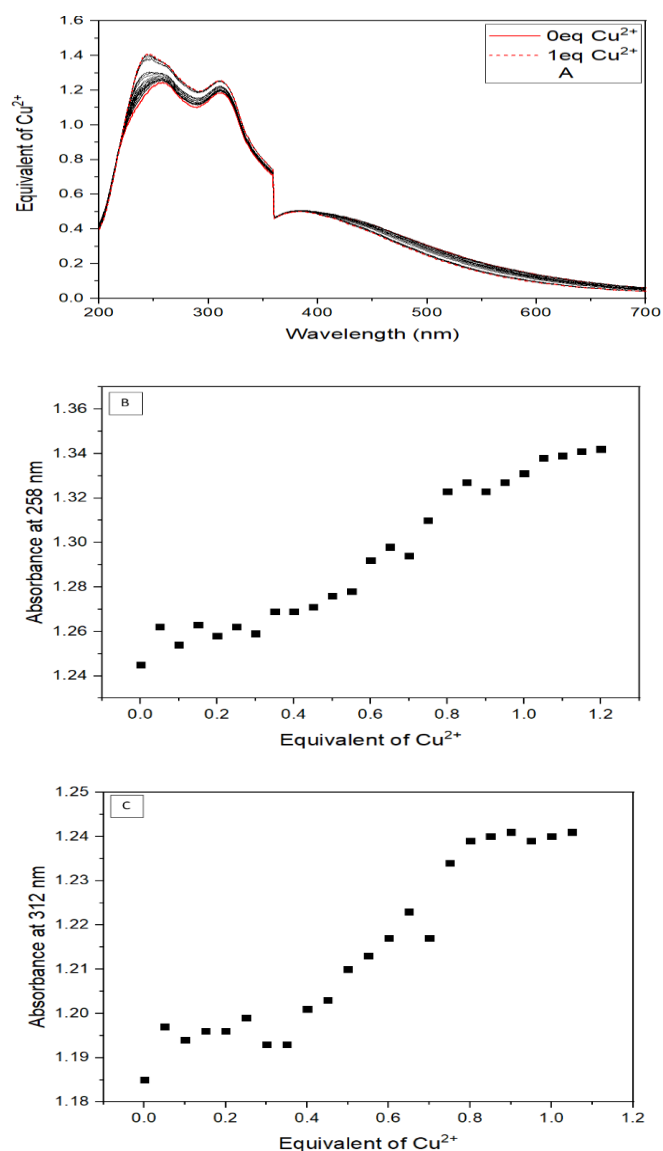


FIGURE 15 [A]: UV-visible absorption spectroscopy titration of 0.07 mM $C_1V^{2+}AN-Cl.2PF_6^-$ with 50 mM $[Cu(BF_4)_2.6H_2O]$ [B], and [C]: plots of absorbances at 258 nm and 312 nm, respectively, versus added equivalents of Cu^{2+} ion at r.t using quartz cell with a path length of 1 cm

The 0.07 mM $C_1V^{2+}AN-Cl.2PF_6^-$ solution was titrated with 50 mM of $Fe(BF_4)_2.6H_2O$ in ACN and followed by absorption spectroscopy, as shown in Figure 16 (A). The recorded absorptions at 275 nm, 311 nm, and

385 nm of this solution against different amount of added metal ion are plotted and presented in Figures 16 (B, C, and D). Similar notes and results appeared like those in case of titration with Zn^{2+} ion.

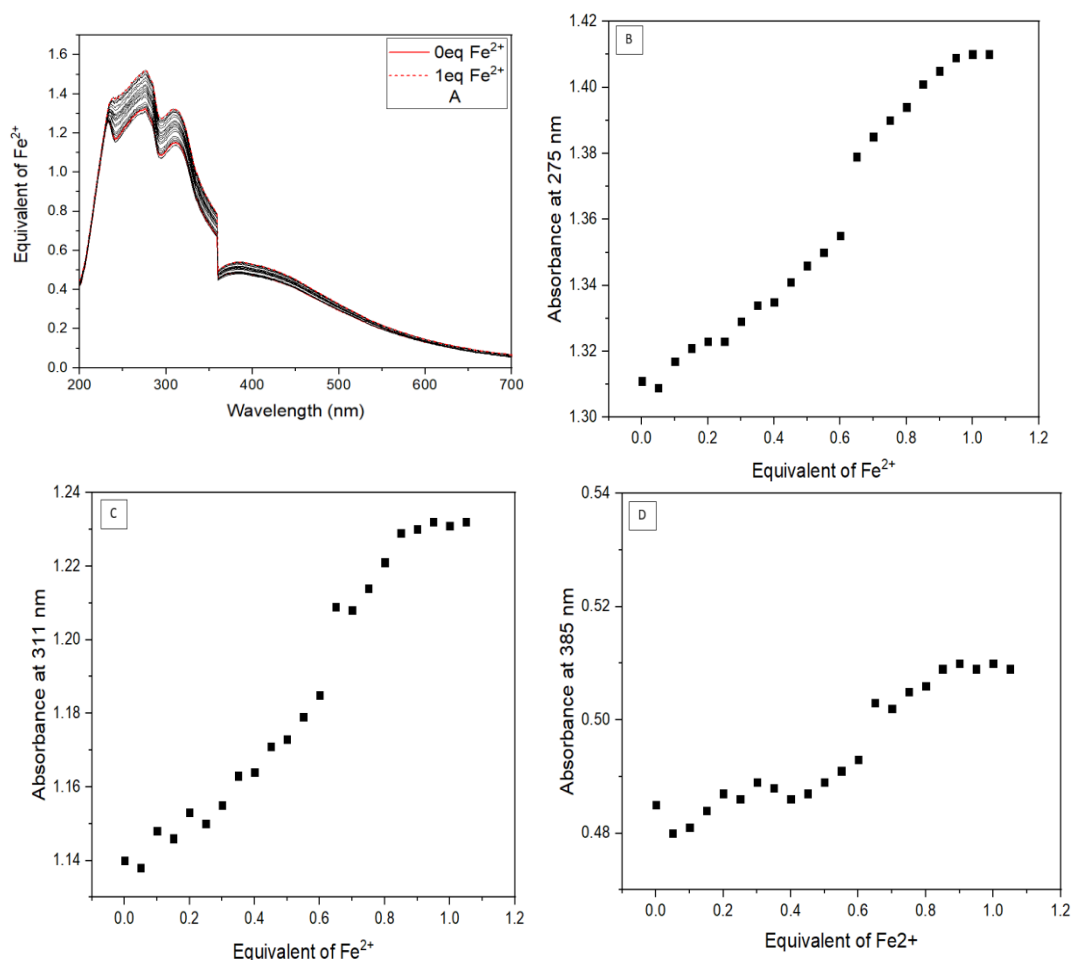
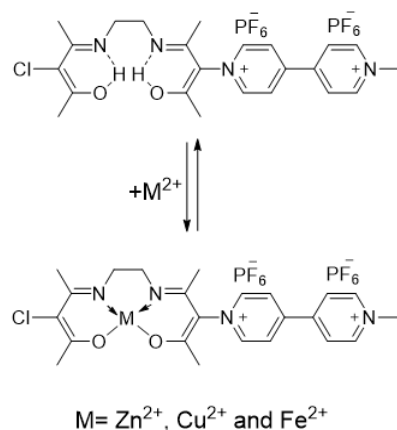


FIGURE 16 [A]: UV-visible absorption spectroscopy titration of 0.07 mM $C_1V^{2+}AN-Cl.2PF_6^-$ with 50 mM $[Fe(BF_4)_2.6H_2O]$ [B], [C], and [D]: plots of absorbances at 258 nm, 312 nm, and 385 nm, respectively, versus added equivalents of Fe^{2+} ion at r.t using quartz cell with a path length of 1 cm



SCHEME 3 Proposed structures of $M-C_1V^{2+}AN-Cl.2PF_6^-$ complexes

Conclusion

In solution, Zn^{2+} , Cu^{2+} , and Fe^{2+} complexes with $C_1V^{2+}AN-Cl.2PF_6^-$ are prepared. The Zn^{2+} , Cu^{2+} , and Fe^{2+} complexes with $C_1V^{2+}AN-$

$Cl.2PF_6^-$ are characterized by UV-Visible absorption spectroscopy. The metal ligand ratio is 1:1. We also achieved the main target of this thesis which is the design of one novel molecular switch. Switching from dicationic

viologen $C_1V^{2+}AN-Cl.2PF_6^-$ and $M^{2+}-C_1V^{2+}AN-Cl.2PF_6^-$ to intermolecular dimerized viologen $(C_1V^+AN-Cl.2PF_6^-)_2$ and intermolecular dimerized complexes $(M^{2+}-C_1V^+AN-Cl.2PF_6^-)_2$.

Acknowledgements

The financial support for this research was provided by Ministry of Higher Education Malaysia under FRGS Grant no. 2019-0147-103-02.

Conflict of Interest

The authors declare that there is no conflict of interest.

Orcid:

A. Jassem Israa:

<https://orcid.org/0000-0002-9609-0498>

S. Abdul-Hassan Wathiq:

<https://orcid.org/0000-0003-1297-3822>

A. Flafel Ibrahim:

<https://orcid.org/0000-0002-9407-4996>

References

- [1] P.M.S. Monk, The viologens, physicochemical properties, *Synthesis and Applications of the Salts of*, **1999**, 4. [[Google Scholar](#)], [[Publisher](#)].
- [2] S. Andersson, D. Zou, R. Zhang, S. Sun, L. Sun, Light driven formation of a supramolecular system with three CB [8] s locked between redox-active Ru (bpy) 3 complexes, *Org. Biomol. Chem.*, **2009**, 7, 3605-3609. [[crossref](#)], [[Google Scholar](#)], [[Publisher](#)].
- [3] H. Chen, L. Jia, J. Yao, J. Hu, K. Chen, Z. Chen, H. Li, The relationships of catalytic activity of metal Schiff base catalysts and the Hammett constants of their anion-cationic substituents on ligand, *J. Phys. Org. Chem.*, **2015**, 28, 570-574. [[crossref](#)], [[Google Scholar](#)], [[Publisher](#)].
- [4] A. Iordache, M. Oltean, A. Milet, F. Thomas, B. Baptiste, E. Saint-Aman, C. Bucher, Redox control of rotary motions in ferrocene-based elemental ball bearings, *J. Am. Chem. Soc.*, **2012**, 134, 2653-2671. [[crossref](#)], [[Google Scholar](#)], [[Publisher](#)].
- [5] R. Kannappan, C. Bucher, E. Saint-Aman, J.C. Moutet, A. Milet, M. Oltean, E. Metay, S. Pellet-Rostaing, M. Lemaire, C. Chaix, Viologen-based redox-switchable anion-binding receptors, *New. J. Chem.*, **2010**, 34, 1373-1386. [[crossref](#)], [[Google Scholar](#)], [[Publisher](#)].
- [6] K. Ueno, A.E. Martell, Ultraviolet and Visible Absorption Spectra of Metal Chelates of Bisacetylacetonethylenediimine and Related Compounds, *J. phys. Chem.*, **1957**, 61, 257-261. [[crossref](#)], [[Google Scholar](#)], [[Publisher](#)].
- [7] A.H. Kianfar, S. Zargari, Synthesis, spectroscopy and electrochemical study of cobalt (III) N_2O_2 Schiff-base complexes, *J. Coord. Chem.*, **2008**, 61, 341-352. [[crossref](#)], [[Google Scholar](#)], [[Publisher](#)].
- [8] M. Saeed, Z. Khalid, R. Saleem, Synthesis and chemical characterization of metals (Al, Cr, Co, Mn and VO) complexes with acetylacetonone (β -diketone), *J. Nat. Sci. Res.*, **2017**, 7, 49-55. [[Pdf](#)], [[Publisher](#)].
- [9] M. Otaghi, M. Azami, A. Khorshidi, M. Borji, Z. Tardeh, The association between metabolic syndrome and polycystic ovary syndrome: a systematic review and meta-analysis, *Metab. Syndr.: Clin. Res. Rev.*, **2019**, 13, 1481-1489. [[crossref](#)], [[Google Scholar](#)], [[Publisher](#)].
- [10] Y.Y. Chen, D.E. Chu, B.D. McKinney, L.J. Willis, S.C. Cummings, High-spin, five-coordinate complexes of cobalt (II), nickel (II), and copper (II) with linear, pentadentate keto, iminato ligands, *Inorg. Chem.*, **1981**, 20, 1885-1892. [[crossref](#)], [[Google Scholar](#)], [[Publisher](#)].
- [11] A.H. Kianfara, S. Zargari, H.R. Khavasi, Synthesis and electrochemistry of M (II) $N_2 O_2$ schiff base complexes: X-Ray structure of {Ni [Bis (3-chloroacetylaceton) ethylenediimine]}, *J. Iran. Chem. Soc.*, **2010**, 7, 908-916. [[crossref](#)], [[Google Scholar](#)], [[Publisher](#)].

- [12] Y. Fujii, An NMR study of metal complexes containing acetylacetonate and related compounds. I. The Preparation, Halogenation and NMR Spectra of Cobalt (III) Complexes Containing Acetylacetonate and Bis (acetylacetonate) ethylenediimine, *Bull. Chem. Soc. Jpn.*, **1970**, *43*, 1722-1728. [[crossref](#)], [[Google Scholar](#)], [[Publisher](#)].
- [13] A. Kumar, S.D. Kurbah, I. Syiemlieh, S.A. Dhanpat, R. Borthakur, R.A. Lal, Synthesis, characterization, reactivity, and catalytic studies of heterobimetallic vanadium (V) complexes containing hydrazone ligands, *Inorganica Chim. Acta*, **2021**, *515*, 120068. [[crossref](#)], [[Google Scholar](#)], [[Publisher](#)].
- [14] M.R. Maurya, S. Khurana, W. Zhang, D. Rehder, Biomimetic oxo-, dioxo- and oxo-peroxo-hydratonato-vanadium(IV/V) complexes, *J. Chem. Soc., Dalton Trans.*, **2002**, *15*, 3015-3023. [[crossref](#)], [[Google Scholar](#)], [[Publisher](#)].
- [15] C.K. Chou, Y.T. Chang, M. Korinek, Y.T. Chen, Y.T. Yang, S. Leu, I.L. Lin, C.J. Tang, C.C. Chiu, The regulations of deubiquitinase USP15 and its pathophysiological mechanisms in diseases, *Int. J. Mol. Sci.*, **2017**, *18*, 902. [[crossref](#)], [[Google Scholar](#)], [[Publisher](#)].
- [16] E.J. Park, B.C. Park, Y.J. Kim, A. Canlier, T.S. Hwang, Elimination and substitution compete during amination of poly (vinyl chloride) with ethylenediamine: XPS analysis and approach of active site index, *Macromol. Res.*, **2018**, *26*, 913-923. [[crossref](#)], [[Google Scholar](#)], [[Publisher](#)].
- [17] A. Cuevas, I. Viera, M.H. Torre, E. Kremer, Susana; Etcheverry; Enrique, *Acta Farnz. Borlaerense*, **2008**.
- [18] D.A. Köse, H. Necefoğlu, Synthesis and characterization of bis (nicotinamide) m-hydroxybenzoate complexes of Co (II), Ni (II), Cu (II) and Zn (II), *J. Therm. Anal. Calorim.*, **2008**, *93*, 509-514. [[crossref](#)], [[Google Scholar](#)], [[Publisher](#)].
- [19] T. Kurauchi, M. Matsui, Y. Nakamura, S.I. Ooi, S. Kawaguchi, H. Kuroya, Six-coordinate copper (II) complexes derived from the reactions of bis (acetylacetonate)-and bis (ethyl acetoacetato)-copper (II) with some bidentate nitrogen bases, *Bull. Chem. Soc. Jpn.*, **1974**, *47*, 3049-3056. [[crossref](#)], [[Google Scholar](#)], [[Publisher](#)].
- [20] R.M. Badger, The relation between the internuclear distances and force constants of molecules and its application to polyatomic molecules, *J. Chem. Phys.*, **1935**, *3*, 710-714. [[crossref](#)], [[Google Scholar](#)], [[Publisher](#)].
- [21] E. Krishnamoorthy, V. Sugumaran, R. Gosala, B. Purushothaman, B. Subramanian, Influence of varying thermal treatment on bioactive material with equal Ca/P ratio: A local drug delivery system for bone regeneration, *J. Biomed. Mater. Res. Part B Appl. Biomater.*, **2023**, *111*, 402-415. [[crossref](#)], [[Google Scholar](#)], [[Publisher](#)].
- [22] D. Trache, Comments on "Effect of hydrolysed cellulose nanowhiskers on properties of montmorillonite/poly(lactic acid) nanocomposites" By Reza Arjmandi et al., *Int. J. Biol. Macromol.*, **2016**, *88*, 497-498. [[crossref](#)], [[Google Scholar](#)], [[Publisher](#)].
- [23] D. Trache, Comments on "thermal degradation behavior of hypochlorite-oxidized starch nanocrystals under different oxidized levels", *Carbohydr. Polym.*, **2016**, *151*, 535-537. [[crossref](#)], [[Google Scholar](#)], [[Publisher](#)].
- [24] V. Kumar, G.M. Sai, R. Verma, K.R. Mitchell-Koch, D. Ray, V.K. Aswal, P. Thareja, K. Kuperkar, P. Bahadur, Tuning cationic micelle properties with an antioxidant additive: a molecular perspective, *Langmuir*, **2021**, *37*, 4611-4621. [[crossref](#)], [[Google Scholar](#)], [[Publisher](#)].
- [25] V.V. Seminko, P.O. Maksimchuk, N.V. Kononets, E.N. Okrushko, I.I. Bepalova, A.A. Masalov, Y.V. Malyukin, Y.I. Boyko, Luminescence of F0 centers in CeO₂ nanocrystals, *PACS*, **2016**, 20-23. [[Google Scholar](#)], [[Publisher](#)].
- [26] T. Sakano, F. Ito, T. Ono, O. Hirata, M. Ozawa, T. Nagamura, Synthesis and electrochromic properties of a highly water-soluble hyperbranched polymer viologen,

- Thin Solid Films*, **2010**, *519*, 1458-1463. [[crossref](#)], [[Google Scholar](#)], [[Publisher](#)].
- [27] PHD W.S. Abdul-hassan, Thesis, Université Grenoble Alpes), **2018**.
- [28] X. Liu, K.G. Neoh, L. Zhao, E.T. Kang, Surface functionalization of glass and polymeric substrates via graft copolymerization of viologen in an aqueous medium, *Langmuir*, **2002**, *18*, 2914-2921. [[crossref](#)], [[Google Scholar](#)], [[Publisher](#)].
- [29] A. Iordache, M. Retegan, F. Thomas, G. Royal, E. Saint-Aman, C. Bucher, Redox-responsive porphyrin-based molecular tweezers, *Chem. Eur. J.*, **2012**, *18*, 7648-7653. [[crossref](#)], [[Google Scholar](#)], [[Publisher](#)].
- [30] V. Iuliano, P. Della Sala, C. Talotta, L. Liguori, G. Monaco, E. Tiberio, C. Gaeta, P. Neri, Chromogenic properties of p-pyridinium-and p-viologen-calixarenes and their cation-sensing abilities, *J. Org. Chem.*, **2021**, *86*, 13001-13010. [[crossref](#)], [[Google Scholar](#)], [[Publisher](#)].
- [31] W.S. Abdul-Hassan, E. Saint-Aman, G. Royal, C. Kahlfuss, C. Bucher, Molécules et matériaux moléculaires redox-et photo-stimulables, *L'Actualité Chimique*, **2018**, 79-84. [[Google Scholar](#)], [[Publisher](#)].
- [32] J. Courtois, B. Wang, W.S. Abdul-Hassan, L. Almásy, M. Yan, G. Royal, Redox-responsive colloidal particles based on coordination polymers incorporating viologen units, *Inorg. Chem.*, **2020**, *59*, 6100-6109. [[crossref](#)], [[Google Scholar](#)], [[Publisher](#)].
- [33] T. Sakano, F. Ito, T. Ono, O. Hirata, M. Ozawa, T. Nagamura, Synthesis and electrochromic properties of a highly water-soluble hyperbranched polymer viologen, *Thin Solid Films*, **2010**, *519*, 1458-1463. [[crossref](#)], [[Google Scholar](#)], [[Publisher](#)].
- [34] C. Kahlfuss, A. Milet, J. Wytko, J. Weiss, E. Saint-Aman, C. Bucher, Hydrogen-Bond Controlled π -Dimerization in Viologen-Appended Calixarenes: Revealing a Subtle Balance of Weak Interactions, *Org. Lett.*, **2015**, *17*, 4058-4061. [[crossref](#)], [[Google Scholar](#)], [[Publisher](#)].
- [35] J. Ding, C. Zheng, L. Wang, C. Lu, B. Zhang, Y. Chen, M. Li, G. Zhai, X. Zhuang, Viologen-inspired functional materials: synthetic strategies and applications, *J. Mater. Chem. A*, **2019**, *7*, 23337-23360. [[crossref](#)], [[Google Scholar](#)], [[Publisher](#)].
- [36] A. Juneau, M. Frenette, Exploring curious covalent bonding: Raman identification and thermodynamics of perpendicular and parallel pancake bonding (pimers) of ethyl viologen radical cation dimers, *J. Phys. Chem. B*, **2021**, *125*, 10805-10812. [[crossref](#)], [[Google Scholar](#)], [[Publisher](#)].
- [37] R. Dobrawa, F. Würthner, Photoluminescent supramolecular polymers: metal-ion directed polymerization of terpyridine-functionalized perylene bisimide dyes, *Chem. Commun.*, **2002**, 1878-1879. [[crossref](#)], [[Google Scholar](#)], [[Publisher](#)].

How to cite this article: Israa. A. Jassem*, Wathiq S. Abdul-Hassan, Ibrahim A. Flafel. Novel molecular switches based on viologen ligand and its transition metal complexes. *Eurasian Chemical Communications*, 2023 5(9), 758-775. **Link:** https://www.chemcom.com/article_171848.html